Available online at www.sciencedirect.com
ScienceDirect
European Journal of Mechanics B/Fluids 27 (2008) 491–500

A numerical study of flows driven by a rotating magnetic field in a square container

Karel Fraňa [a,*], Jörg Stiller [b]

[a] *Technical University of Liberec, Department of Power Engineering Equipment, Czech Republic*
[b] *Institute for Aerospace Engineering (ILR), Technische Universität Dresden, D-01062 Dresden, Germany*

Received 18 October 2006; received in revised form 9 September 2007; accepted 9 October 2007

Available online 18 October 2007

Abstract

The magnetically induced fluid flow in a square container is investigated by means of numerical simulations. Low frequency/ low induction conditions are assumed. The effect of the rotating magnetic field gives rise to a time-independent magnetic body force, computed via the electrical potential equation and Ohm's law and a time-dependent part that is neglected due to the low-interaction parameter. The magnetic body force calculation is verified successfully by comparison with the exact solution. The behavior of the fluid flow in the square container reveals similar features to the flow in the cylindrical container, for instance, in the dependence on the intensities of the magnetic field. However, we did find differences in the velocity field distribution. Particularly, in the finite as well as infinite geometry, the velocity field is influenced by the corner of the container and remains non-axisymmetric in a wide range of Taylor numbers.

Keywords: Numerical methods; Simulation; Rotating magnetic field; Square container; Magnetic body force

1. Introduction

The stirring of electrically conducting fluids by a rotating magnetic field (RMF) is an attractive way to control fluid motion without any direct contact with this fluid. This advantage has incited to apply this technique in applications of crystal growth and metallurgical processes. The present knowledge of magnetically induced flow is constrained predominately to cylindrical containers. For this geometry, various flow regimes in the dependence on the intensity of the magnetic field and the container size were identified numerically [1–5] and proved experimentally [6,24]. From a practical point of view, the most important change of the flow regime is associated with the instability threshold at which the symmetry of the main rotating flow is disrupted and the azimuthal as well as the secondary meridional flow started to fluctuate chaotically in time and space [7]. For the results of the 2d linear stability analysis we refer to [8–10] and for the 3d stability analysis to [11,12]. By means of the stability analysis, the critical Taylor number was identified, which practically divides the magnetically induced flow into a subcritical and a supercritical flow regime. In the supercritical flow regime, this flow is governed by Taylor–Görtler type vortices [13]. To visualize these

* Corresponding author.
E-mail address: karel.frana@seznam.cz (K. Fraňa).

0997-7546/$ – see front matter
doi:10.1016/j.euromechflu.2007.10.001

vortices, techniques such as the secondary invariant or the vortices of the fluctuating velocity field were adopted successfully [14]. The results of the main flow based on the numerical and experimental observations were reported in [7].

This paper deals with the numerical study of the flow driven by the RMF in the square container. In consideration of previous results, we compare the results in the cylindrical and square container in respect to the body force and the induced flow. In the calculation of the magnetic force, we consider low frequency/ low induction conditions. Under these conditions, the magnetic force distribution is computed via the electrical potential equation and the Ohm's law. The validation of the magnetic force calculation is presented. However, the main focus is concentrated on the resulted flow described in consideration to the shape geometry and the intensity of the RMF.

The paper is organized as follows: in Section 2, methods of the magnetic body force calculation as well as governed flow equations are introduced. The computational code and required code validations are described in Section 3. Section 4 reports on the flow behavior and the main differences between the flow in the square and cylindrical container.

2. Mathematical model

A square container, bound by electrically insulated walls with the side length $2L$ and the height H, is filled by an electrically conducting fluid with density ρ, kinematical viscosity ν and electrical conductivity σ. The fluid inside is stirred by a rotating magnetic field with the magnetic induction $\vec{B}$ and the constant angular frequency ω. The principal effect of the RMF is the induction of a rotating flow in the azimuthal direction. Furthermore, due to the imbalance between the magnetic body force and the pressure, a weaker secondary flow is generated in the vertical direction. Fig. 1 shows a sketch of the problem.

The flow is governed by the Navier–Stokes equations for incompressible viscous flows,

$$\frac{\partial \vec{u}}{\partial t} + \nabla \cdot \vec{u}\vec{u} = -\nabla p + \nabla^2 \vec{u} + \vec{f}, \tag{1}$$

$$\nabla \cdot \vec{u} = 0 \tag{2}$$

where the velocity $\vec{u}$ and time t are scaled by ν/L, L^2/ν and the pressure p by $\rho\nu^2/L^2$ and an external mean body force $\vec{f}$ are scaled by $\rho\nu^2/L^3$. For the calculation of the magnetic body force, the low-frequency and the low-induction RMF condition are assumed. To satisfy these considerations, the magnetic Reynolds number Rm and the shielding parameter S have to be in relation that $Rm = \mu\sigma u R \ll S = \mu\sigma\omega R^2 < 1$, where μ denotes the magnetic

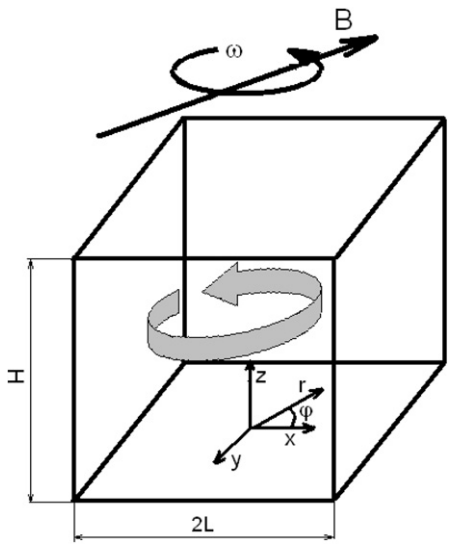

Fig. 1. Sketch of the solved problem with the depiction of the fluid flow orientation.

permeability. The non-dimensional induction, which is scaled by B_0, is defined in the Cartesian coordinate system as follows

$$\vec{B} = [\cos \omega t \vec{e}_y - \sin \omega t \vec{e}_x] \tag{3}$$

where $\vec{e}_x$ and $\vec{e}_y$ are unit vectors. Using Ohm's law, the body force takes the form

$$\vec{f} = 2Ta(\vec{j} \times \vec{B}) = 2Ta\left[\left(-\nabla \Phi - \frac{\partial \vec{A}}{\partial t} + \vec{u} \times \vec{B}\right)\right] \times \vec{B} \tag{4}$$

where Φ, $\vec{A}$ and $\vec{j}$ are the dimensionless electric potential, vector potential and current density, scaled by $\omega_0 B_0 L^2$, $B_0 L$ and $\sigma \omega_0 B_0 L$, respectively. The magnetic Taylor number is defined as follows

$$Ta = \frac{\sigma \omega B_0^2 L^4}{2\rho \nu^2}. \tag{5}$$

In the case of low-frequency and the low-induction conditions, the term $\vec{u} \times \vec{B}$ can be neglected and the term of the partial time derivation of the magnetic vector potential (Eq. (6)) is derived under the conditions of $\nabla \cdot \vec{A} = 0$ and $\vec{B} = \nabla \times \vec{A}$.

$$\frac{\partial \vec{A}}{\partial t} = -\omega[x \sin \omega t - y \cos \omega t]\vec{e}_z. \tag{6}$$

To determine the electric potential Φ in Eq. (4), we can exploit that $\nabla \cdot \vec{j} = 0$ and at boundaries $\vec{j} \cdot \vec{n} = 0$. Thus, the equation for electric potential derived on the basis of Ohm's law is of the form

$$\nabla^2 \cdot \Phi = -\nabla \cdot \left(\frac{\partial \vec{A}}{\partial t}\right) = 0 \tag{7}$$

with the Neumann condition

$$\frac{\partial \Phi}{\partial n} = -\frac{\partial A_n}{\partial t}. \tag{8}$$

For the infinite-length container, this equation simplifies to $\partial \Phi / \partial n = 0$.

Practically, the time-dependent Lorentz force distribution is computed using Eqs. (4), (7) and (8). Nevertheless, the body force can be divided further into two parts; the time-dependent and the mean part, respectively. Under considerations that the interaction parameter is $N = \sigma B^2 / \rho \omega \ll 1$ only the mean part of the magnetic body force has a significant effect on the magnetically induced fluid flow and the fluctuating part can be neglected [15,16]. The time-averaged part is defined as follows

$$\vec{f}_{\text{avg}} = \frac{1}{T} \int_0^{\pi/\omega} \vec{f}\, dt = \frac{1}{N} \sum_{i=1}^{N} \vec{f}_i \tag{9}$$

where N denotes the number of regularly distributed samples used for the time averaging within the half period of the magnetic field oscillation. The influence of the parameter N on the accuracy of the magnetic Lorentz force calculation is discussed in the next section.

The size of the container is denoted using an aspect ratio Z expressing the ratio between the height and the side length ($Z = H/2L$) of the container.

3. Numerical method

The numerical study of the magnetically driven flow is carried out using a self-developed code in which the pressure-stabilized Petrov–Galerkin discretization method based on linear shape functions was applied [17]. To solve the coupled velocity and pressure in the Navier–Stokes equation, the splitting approach was adopted which leads to an implicit Poisson type equation for the pressure and an explicit predictor-corrector step for the velocity. For the predictor step, the Jacobi iterations are applied but for the pressure equation, the more effective CG solver is preferred instead. The time-dependent term was discretized by means of the Adam–Bashforth schema. The numerical model

was implemented on top of the MG grid library [18,19], which provides data structures, the handling of the unstructured grids and methods for grid adaptations. The parallelization with the MG library is based on a grid partitioning providing the decomposition of the computational grid into a specific number of partitions. The test of the parallel efficiency was carried out on the cylindrical cavity flow driven by RMF and the results were discussed in [19]. In the same reference, the details about the mathematical formulation are given.

The code was validated on several tests including a transient channel flow or a flow driven by the rotating magnetic field in the laminar Stokes regime. The convergence study proved the second order accuracy in time and space [19]. In the transient flow regime, the code was validated using the linear stability analysis carried out in the flow driven by the rotating and traveling magnetic field. The results were in good agreement with published results by Grants and Gerbeth [11,25]. The magnetically induced flow, solved numerically, was compared with experiments demonstrating further successful agreements in the velocity field and turbulent properties. For details we refer to [7].

In the continued validation process discussed further, we focus on the test of the mathematical model used for the calculation of the magnetic body force distribution. This mathematical model, introduced above, is adopted from the RMF flow problem in the cylindrical container with the aspect ratio of infinite and finite units. For all aspect ratios, the exact analytical form of the magnetic body force distribution for the RMF is well known [20]. By comparison with computed results, the deviation, based on the maximum norm, is found in the order of 10^{-4}. To evaluate this magnitude, it must be considered that the deviation of the velocity field was resolved in the order of 10^{-3} [19]. Because of the coupling between the inaccuracy in the velocity and the magnetic field computation, we fulfill a condition that the inaccuracy in the magnetic field is lower compared to that found in the velocity field.

The efficiency and the accuracy of averaging tools, applied for the determination of the mean magnetic body force, is tested for the case of the square container of an infinite length. As a reference case, the force distribution averaged by 100 samples at the half time period of the magnetic field oscillation was computed. The deviations in respect to various numbers of samples are summarized in Table 1.

This validation reveals that we need at least 16 samples to average the time-dependent force in order to reduce the inaccuracies lying below the order of 10^{-7}. Considering this conclusion, corresponding contours of the magnetic body force for the aspect ratios one are depicted in Fig. 2. The computational grid is quasi equidistant and consists

Table 1
The absolute values of computed deviations in the magnetic body force calculations in respect to various numbers of samples in the averaging process

$\frac{f_1-f_{100}}{f_1}$	$\frac{f_2-f_{100}}{f_2}$	$\frac{f_4-f_{100}}{f_4}$	$\frac{f_8-f_{100}}{f_8}$	$\frac{f_{16}-f_{100}}{f_{16}}$	$\frac{f_{32}-f_{100}}{f_{32}}$	$\frac{f_{64}-f_{100}}{f_{64}}$
1	1	5.7×10^{-6}	3.18×10^{-6}	8.7×10^{-8}	8.3×10^{-8}	under 10^{-8}

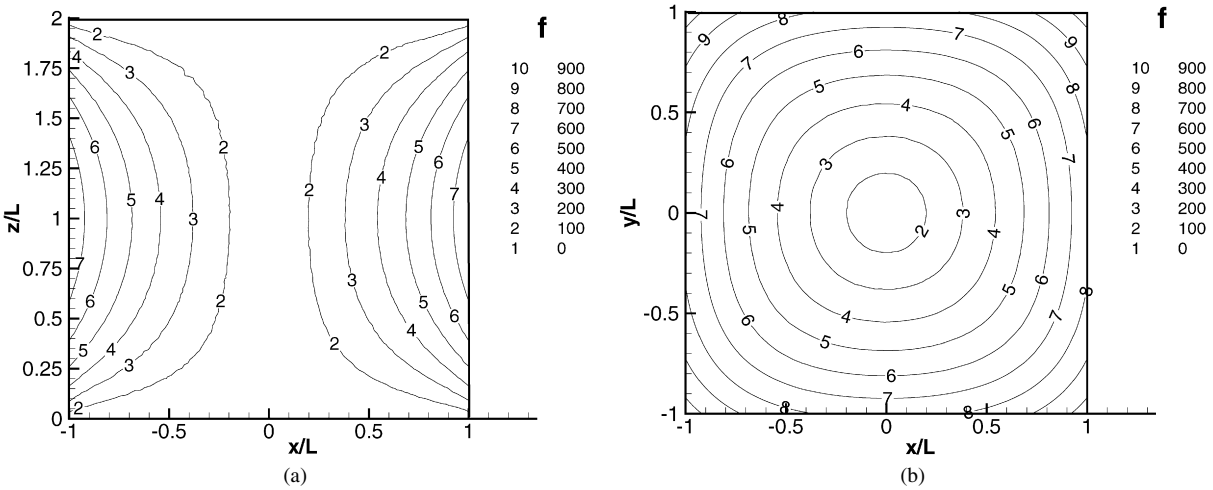

(a) (b)

Fig. 2. Contours of the magnetic body force distribution at the Taylor number 1×10^3 and for the finite-length square container defined by the aspect ratio one (a) in the meridional and (b) horizontal slice.

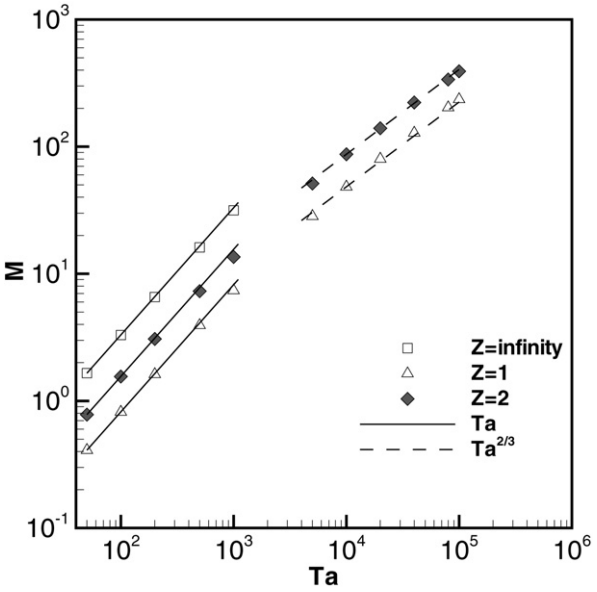

Fig. 3. Dependence the angular momentum on the Taylor number for aspect ratios infinity, one and two.

of 3.5×10^6 tetrahedral cells for the aspect ratio one and 6.4×10^6 for the aspect ratio two, respectively, with a grid spacing of approximately $1/40$.

4. Results

According to previous works [1,16,5] carried out in the cylindrical container, the RMF intensity had a critical influence on the resulting flow regime. It has been found that the maximum of the azimuthal velocity of the melts increases linear with the Taylor number in the range of low Taylor numbers. For higher Taylor numbers, the maximum azimuthal velocity increases by $Ta^{2/3}$. This dependency at a higher Taylor number is caused by the behavior of the boundary layer flow. Qualitatively, the same results can be found considering the angular momentum of the azimuthal velocity. Fig. 3 shows the dependence the angular momentum on the Taylor number in the square container, where the volume-averaged angular momentum is computed as

$$M = \frac{1}{V} \int_{\Omega} u_{\varphi} r \, d\Omega \tag{10}$$

where V denotes the volume of the container. The dependence of the angular momentum on the Taylor number is linear in the range of very low Ta up to approximately $Ta < 1 \times 10^3$. For $Ta \geqslant 1 \times 10^4$, a slope of $2/3$ is determined in the container with the finite length. As mentioned above, this flow behavior depending on Taylor numbers is identical to that observed in the cylindrical container [1,2] and it is fully consistent with Davidson's theory derived from the cylindrical container [21]. Due to the imbalance of the centrifugal force and the radial pressure gradient near the horizontal walls, the Ekman pumping appears and causes the redistribution of the angular momentum. Besides that, the generated Ekman type layer on the top and bottom walls gives rise to intensive wall friction and consequently the loss of the angular momentum. These two significant effects have a tendency to continuously decrease the intensity of the angular momentum at moderate Taylor numbers. The investigation of the flow in the infinite container was constrained to the laminar regime, i.e. $Ta \leqslant 1 \times 10^3$, which is well below the critical Taylor number for the infinite cylinder [22].

The results of the flow stability analysis carried out on the axisymmetric cavity can be used to compare with the results in the non-axisymmetric cavity. In the square container of the aspect ratio one, the flow is without any visible instability up to Taylor number 1×10^5. That is consistent well into [9], where the critical Taylor number was identified at $Ta^{\mathrm{cr}} = 1.23 \times 10^5$. In accordance to the same reference, the critical Taylor number was determined at

Table 2
The non-dimensional force momentum at $Ta = 1 \times 10^3$

Aspect ratio Z	infinity	1	2
Integral value	887.44	281.52	457.36

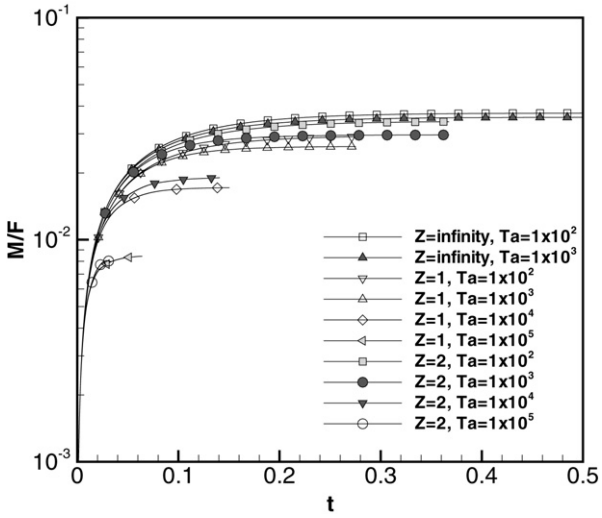

Fig. 4. Development of the angular momentum in time for aspect ratios infinite, one and two.

$Ta^{\mathrm{cr}} = 2.25 \times 10^4$ in the aspect ratio two. In the same size of the non-axisymmetric cavity, the visible flow instabilities occurred somewhere between Taylor numbers 1×10^4 and 1×10^5.

To assume the influence of the size of the container on the intensity of the magnetic body force, the non-dimensional integral of the force momentum scaled by the size of the container defined in Eq. (11) was adopted for the angular momentum evaluation. For instance, values of the non-dimensional force momentum computed at $Ta = 1 \times 10^3$ is summarized in Table 2.

$$F = \frac{1}{V} \int_{\Omega} f_{\varphi} r \, d\Omega. \tag{11}$$

The final results of the velocity field or the angular momentum are obtained after reaching of the developed state in the unsteady flow regime. The condition for this flow state is given by inconsiderable changes e.g. in the global integral of the angular momentum in time. Fig. 4 shows the time dependence of the angular momentum for different Taylor numbers and aspect ratios. The integral of the angular momentum is scaled by taking into account the effect of the magnetic force distribution for the different aspect ratios of the container. The time evaluation of the angular momentum U_{φ} can be closely given by the relation (12) derived in [23] for the spin-up flow in the cylindrical container.

$$U_{\varphi} = \tanh(\pi t / t_{\mathrm{dev}}). \tag{12}$$

The index dev denotes the fully developed flow. On the basis of the evaluation of the angular momentum illustrated in Fig. 4, the required time t_{dev} for reaching a fully developed state can be determined only approximately. For instance, for aspect ratio one and Taylor number 1×10^5, the $t_{\mathrm{dev}}/t_{\mathrm{spin\text{-}up}}$ is estimated at 1.04 where $t_{\mathrm{spin\text{-}up}}$ denotes spin-up time expressed in [23]. Considering the spin-up effect in the axisymmetric cavity, $t_{\mathrm{dev}}/t_{\mathrm{spin\text{-}up}}$ varied between 1.05 and 1.10 and thus the spin-up effect in the axisymmetrical and non-axisymmetrical cavity is very similar.

The distribution of the azimuthal velocity depends on the Taylor number, and as demonstrated further, essentially on the shape of the container. Fig. 5 (a) and (b) show contours of the instantaneous azimuthal velocity at the horizontal slice in the square container of the infinity length. In the whole subcritical regime, the velocity field is affected strongly by the corners of the container, and consequently, we can observe that the flow distribution has four velocity peaks in the azimuthal velocity field.

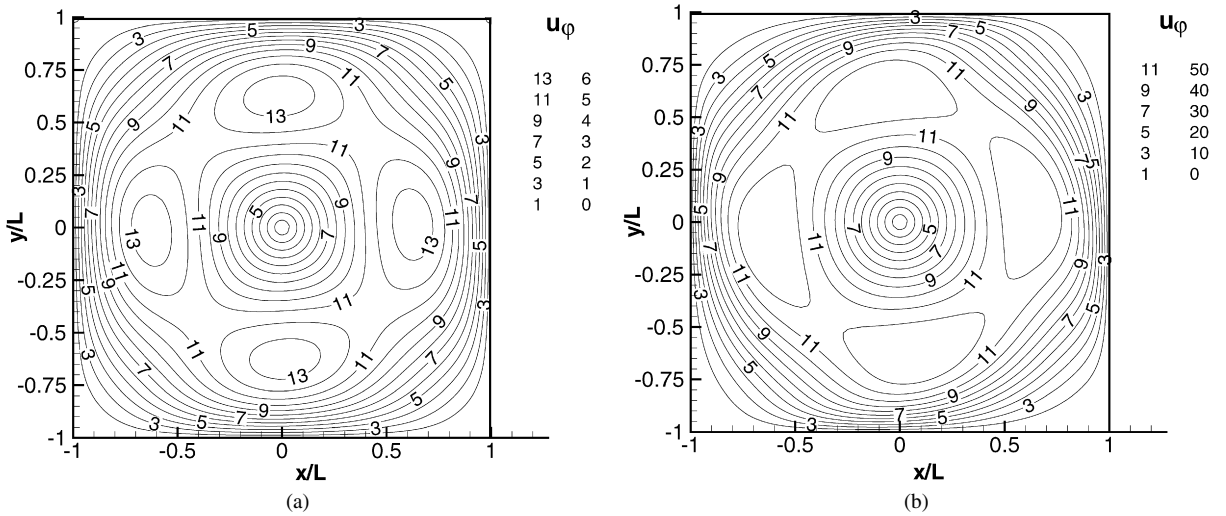

Fig. 5. Contours of the azimuthal velocity for the aspect ratio infinity at Taylor numbers: (a) 1×10^2 and (b) 1×10^3.

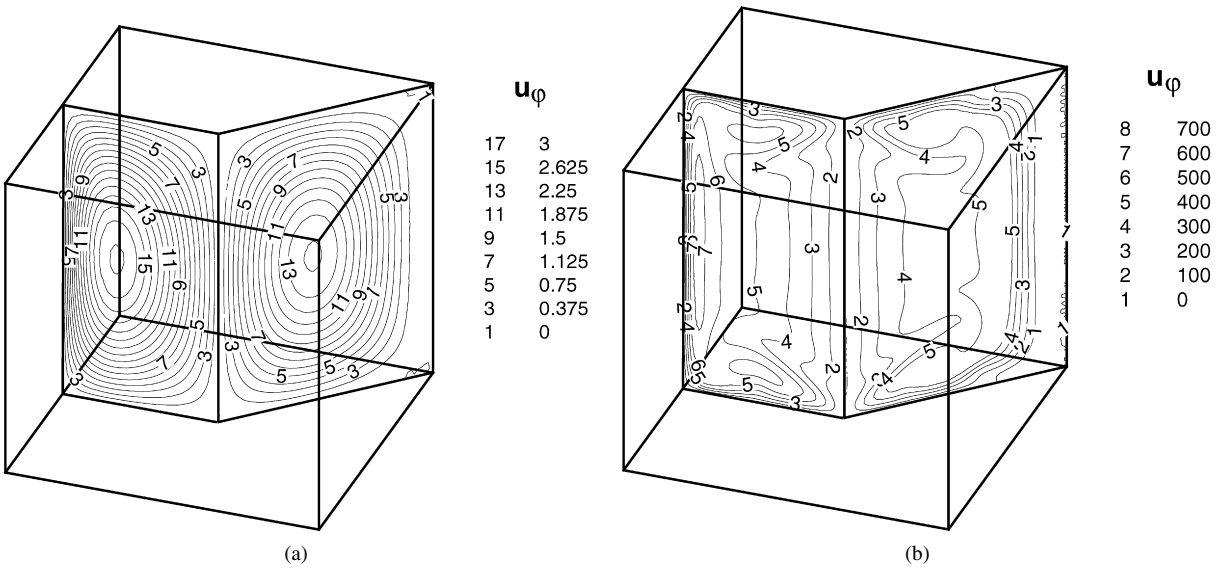

Fig. 6. Contours of the azimuthal velocity in vertical slices for the aspect ratio one and at Taylor numbers: (a) 1×10^2 and (b) 1×10^5.

The effect of end walls on the flow was studied on the finite container. Because of the non-axisymmetric geometry, the velocity field is visualized in the one horizontal slice shown in Fig. 7 (a) and (b) and the two vertical slices in Fig. 6 (a) and (b), respectively. The velocity fields depicted in the horizontal slice show that four velocity peaks are present in the main azimuthal flow for any intensity of the magnetic field. The homogeneously rotating flow, observed in the finite cylinder [1,2] and [8], doesn't exist in the square geometry in the range of Taylor numbers up to 1×10^5. By contrast, in the square geometry, the different location of the maximum azimuthal velocity depends on the Taylor number. Fig. 8 shows the velocity profiles for aspect ratio one in two different directions, from the centre to the median of a wall, and diagonally to one corner of the container, respectively. With increasing Taylor number, the velocity profile is deformed and the maximum shifted outwards to the vertical walls. Similar tendencies in the azimuthal flow behavior were observed in the cylindrical cavity as well [3]. Particularly, in the cylindrical cavity, the maxima of the azimuthal velocity remain constant approximately 0.8 of the radius at moderate Taylor numbers. In the non-axisymmetric cavity, the maximum appears close to the vertical boundaries, particularly 0.92 of the half side length at Ta 1×10^5.

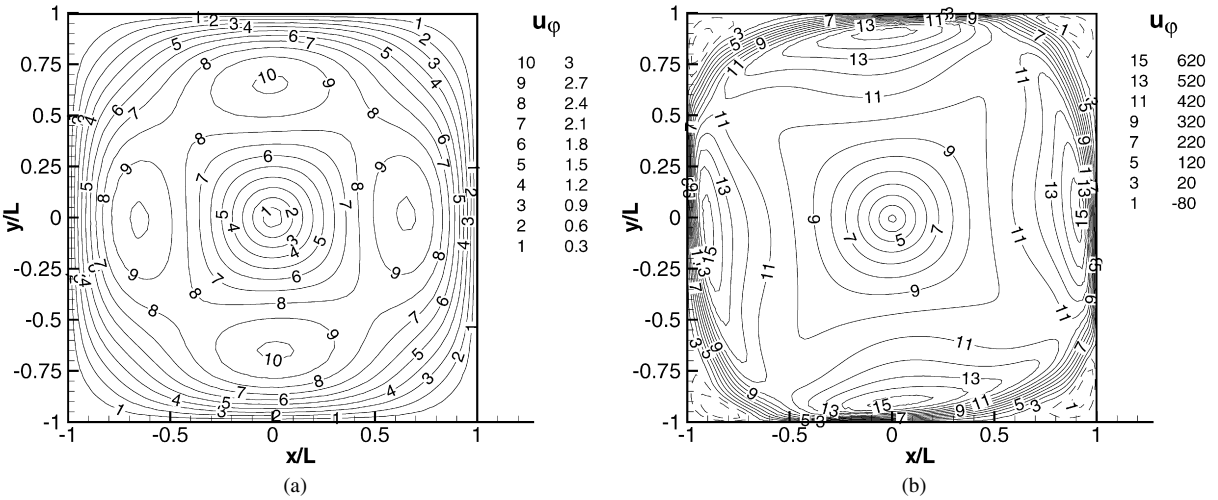

Fig. 7. Contours of the azimuthal velocity in the horizontal slice for the aspect ratio one and at Taylor numbers: (a) 1×10^2 and (b) 1×10^5.

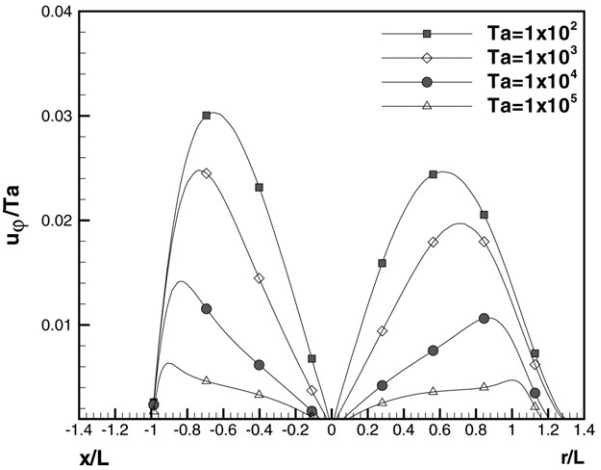

Fig. 8. Velocity profiles in two different directions, from the centre to the median of a wall and diagonally to one corner of the container.

Fig. 9 (a) and (b) show a vector plot of the secondary flow for a aspect ratio one in the steady state and non-linear unsteady flow regime, respectively. In the steady regime, the meridional flow is in the form of the two weak symmetric toriadal vortices and Bödewadt layers at the horizontal boundaries. This structure is identical to that found in the cylindrical cavity [1]. Fig. 9(b) depicts the meridional flow in the inertial non-linear boundary flow regime. This flow is characterized by a solid-body rotation in the flow core and Bödewadt layers at the horizontal boundaries. This picture corresponds to the behavior of the meridional flow in the cylindrical container at the same flow regime [1]. From the point of view of the flow intensity in the vertical direction, the mass transfer due to the meridional flow is intensive in the whole volume of the container in the steady flow regime. However, in the non-linear unsteady flow regime, the meridional flow is intensive at horizontal boundaries and it is weaker inside of the container. The meridional flow behavior is identical to that observed in the cylindrical container [1,2,7].

5. Conclusions

The flow driven by the RMF in a square container was investigated numerically. This flow study was carried out using a computational code in which the time-averaged magnetic body force was computed by means of the electrical potential equation and the Ohm's law. The validation was performed on test cases in which the analytical solution of the magnetic body force distribution is known. The deviation between the exact and the computed magnetic force

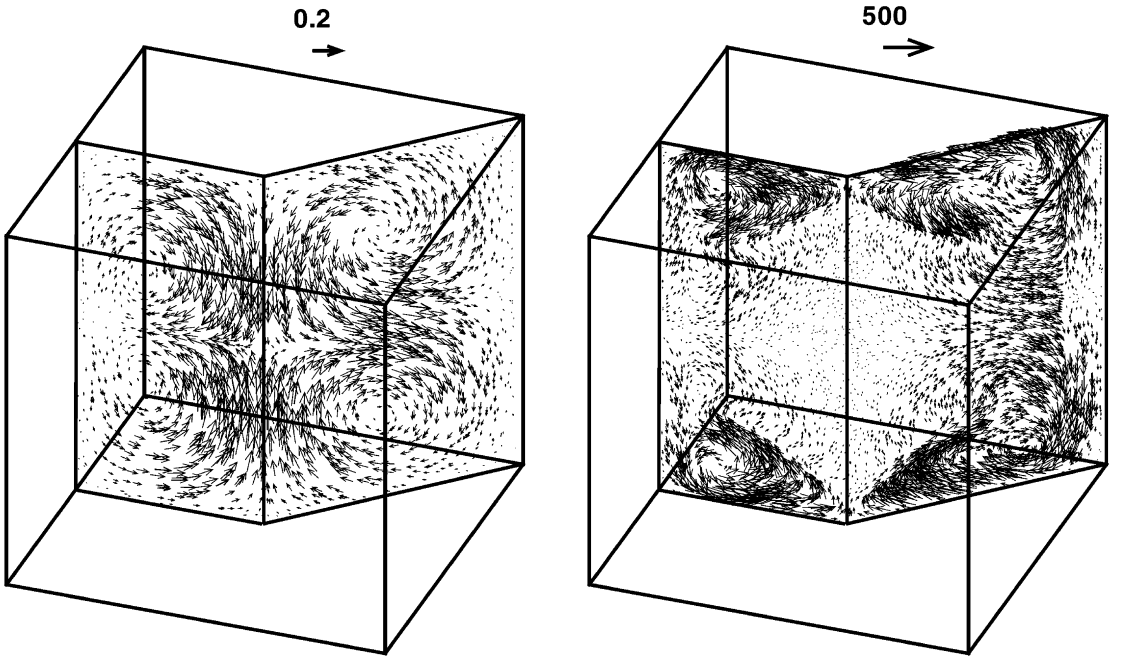

Fig. 9. Vector depiction of the secondary flow for the aspect ratio one and at Taylor numbers: (a) 1×10^2 and (b) 1×10^5.

distribution was negligible in respect to other inaccuracies in the code. The flow study was carried out for aspect ratios one, two at Taylor numbers varied up to 10^5 and for the aspect ratio infinity up to 10^3. The magnetic body force, generating the main swirling flow in the azimuthal direction, has the same form as in the case of the cylindrical container. Even in the non-linear flow regime, the Bödewadt layer at the horizontal boundaries has the same effect as in the axisymmetric cavity. Consequently, similar flow features can be found for the axisymmetric and non-axisymmetric cavity at moderate Taylor numbers, except for the following difference. In the finite container, the non-axisymmetric shape of the cross section leads to a velocity maximum at the median of each side wall whereas the flow is slower near the corners. In the frame of future work, turbulent properties of such flows will be considered to understand more about such flows at moderated Taylor numbers.

Acknowledgements

Financial support from Research Grant MSM 4674788501 and German Deutsche Forschungsgemeinschaft in the frame of the Collaborative Research Center SFB 609 are gratefully acknowledged. We are grateful as well to Dr. Nikrityuk for useful comments.

References

[1] J. Priede, Yu.M. Gelfgat, Numerical simulation of the mhd flow produced by a rotating magnetic field in a cylindrical cavity of finite length, Magnetohydrodynamics 33 (2) (1997) 172–179.
[2] R.U. Barz, G. Gerbeth, U. Wunderwald, E. Buhrig, Yu.M. Gelfgat, Modelling of the isothermal melt flow due to rotating magnetic fields in crystal growth, J. Crystal Growth 180 (1997) 410–421.
[3] L. Martin Witkowski, P. Marty, Effect of a rotating magnetic field of arbitrary frequency on a liquid metal column, Eur. J. Mech. B Fluids 17 (1998) 239–254.
[4] Yu.M. Gelfgat, J. Priede, MHD flows in a rotating magnetic field (a review), Magnetohydrodynamics 31 (1/2) (1995) 188–200.
[5] P.A. Nikrityuk, K. Eckert, R. Grundmann, Numerical study of a laminar melt flow driven by a rotating magnetic field in enclosed cylinders with different aspect ratios, Acta Mech. 186 (2006) 17–35.
[6] M.P. Volz, K. Mazuruk, Flow transitions in a rotating magnetic field, Exp. Fluids 20 (1996) 454–459.
[7] J. Stiller, K. Fraňa, A. Cramer, Transitional and weakly turbulent flow in a rotating magnetic field, Phys. Fluids 19 (2006) 074105.
[8] R. Mößner, G. Gerbeth, Buoyant melt flow under the influence of steady and rotating magnetic fields, J. Crystal Growth 197 (1999) 341–354.

[9] I. Grants, G. Gerbeth, Stability of axially symmetric flow driven by a rotating magnetic field in a cylindrical cavity, J. Fluid Mech. 431 (2001) 407–426.
[10] I. Grants, Yu.M. Gelfgat, Stability of swirling-recirculating flow due to rotating magnetic field, Magnetohydrodynamics 34 (1998) 80–88.
[11] I. Grants, G. Gerbeth, Linear three-dimensional instability of a magnetically driven rotating flow, J. Fluid Mech. 463 (2002) 229–239.
[12] J. S Walker, L. Martin Witkowski, Linear stability analysis for a rotating cylinder with a rotating magnetic field, Phys. Fluids 16 (2004) 2294–2299.
[13] T. Kaiser, K. Benz, Taylor vortex instabilities induced by a rotating magnetic field: A numerical approach, Phys. Fluids 10 (1998) 1104–1110.
[14] K. Fraňa, J. Stiller, R. Grundmann, Taylor–Görtler vortices in the flow driven by a rotating magnetic field in a cylindrical container, J. Visualization 8 (4) (2005) 323–330.
[15] P.A. Davidson, J.C.R. Hunt, Swirling recirculating flow in a liquid–metal column generated by a rotating magnetic field, J. Fluid Mech. 185 (1987) 67–106.
[16] L. Martin Witkowski, J.S. Walker, Nonaxisymmetric flow in a finite-length cylinder with a rotating magnetic field, Phys. Fluids 11 (1999) 1821–1826.
[17] T.J.R. Hughes, L.P. Franca, M. Balestra, A new finite element formulation for computational fluid dynamics, V. Circumventing the Babuška–Brezzi condition: A stable Petrov–Galerkin formulation of the Stokes problem accommodating equal-order interpolations, Comput. Meth. Appl. Mech. Eng. 59 (1986).
[18] J. Stiller, W.E. Nagel, MG – A toolbox for parallel grid adaptation and implementing unstructured multigrid solvers, in: E.H. D'Hollander, et al. (Eds.), Parallel Computing. Fundamentals & Applications, Imperial College Press, 2000.
[19] J. Stiller, K. Fraňa, R. Grundmann, U. Fladrich, W.E. Nagel, A parallel PSPG finite element method for direct simulation of incompressible flow, in: M. Danutello, D. Laforenza, M. Vanneschi (Eds.), Parallel Processing Lecture Notes in Computer Science 3149, Euro-Par 2004, Springer-Verlag, 2004, pp. 726–733.
[20] L.P. Gorbachev, N.V. Nikitin, A.L. Ustinov, Magnetohydrodynamic rotation of an electrically conductive liquid in a cylindrical vessel of finite dimensions, Magnetohydrodynamics 10 (406) (1974) 406–414.
[21] P.A. Davidson, Swirling flow in an axisymmetric cavity of arbitrary profile, driven by a rotating magnetic field, J. Fluid Mech. 245 (1992) 669.
[22] A.T. Richardson, On the stability of a magnetically driven rotating fluid flow, J. Fluid Mech. 63 (1974).
[23] P.A. Nikrityuk, M. Ungarish, K. Eckert, R. Grundmann, Spin-up of a liquid metal flow driven by a rotating magnetic field in a finite cylinder; A numerical and analytical study, Phys. Fluids 17 (2005) 067101.
[24] Yu.M. Gelfgat, L.A. Gorbunov, V. Kolevzon, Liquid metal flow in a finite-length cylinder with a rotating magnetic field, Exp. Fluids 15 (1993) 411–416.
[25] I. Grants, G. Gerbeth, Stability of melt flow due to a traveling magnetic field in a closed ampoule, J. Crystal Growth 269 (2004) 630–638.